Impacts of Fracture Properties on the Formation and Development of Stimulated Reservoir Volume: a Global Sensitivity Analysis

Weiwei Zhu[a], Xupeng He[b], Yiteng Li[b], Gang Lei[c], Ryan Santoso[d], Moran Wang[a,*]

[a] *Department of Engineering Mechanics, Tsinghua University, Beijing, China.*
[b] *Ali I. Al-Naimi Petroleum Engineering Research Center (ANPERC), King Abdullah University of Science and Technology, Thuwal, KSA.*
[c] *Faculty of Engineering, China University of Geosciences, Wuhan, China*
[d] *RWTH Aachen University, Aachen, Germany*

Abstract

Stimulated reservoir volume (SRV), the high-permeable fracture network created by hydraulic fracturing, is essential for fluid production from low-permeable reservoirs. However, the configuration of SRV and its impacting factors are largely unknown. In this work, we adopt the stochastic discrete fracture network method to mimic natural fractures in subsurface formations and conduct a global sensitivity analysis with the Sobol method. The sensitivity of different fracture properties, including geometrical properties (fracture lengths, orientations and center positions), mechanical properties (fracture roughness and fracture strength), fracture sealing properties (probabilities of open fractures and segment lengths) and the fracture intensity, are investigated in two and three-dimensional fracture networks. JRC-JCS model is adopted to identify critically stressed fractures. We find that critically stressed fractures compose the backbone of SRV, while partially open fractures can significantly enlarge the size of SRV by connecting more critically orientated fractures. The fracture roughness is the most influential factor for the total length (area) of critically stressed frac-

*Corresponding author
Email address: mrwang@tsinghua.edu.cn (Moran Wang)

tures. For the relative increase of SRV (RI) in 2D/3D fracture networks, the probability of open fractures is the most significant factor. The fracture lengths and center positions are essential factors for RI in 2D fracture networks but insignificant in 3D fracture networks. This work provides a realistic scenario of the subsurface structure and systematically investigates the influential factors of SRV, which is useful for estimating the size of SRV and predicting shale gas reservoirs' production in an accurate and physically meaningful way.

Keywords

Simulated reservoir volume; Discrete fracture network; Global sensitivity analysis; Geomechanics; Fracture sealing; Geometrical properties

Highlights

- Stimulated reservoir volume (SRV) formed in two and three-dimensional fracture networks are investigated.
- Systematic sensitivity analysis of different fracture properties on the formation and development of SRV is conducted.
- Critically stressed fractures form the backbone of SRV and partially open fractures enlarge the size of SRV significantly.

1. Introduction

In low permeability formations, such as shale reservoirs, natural fractures and hydrofractures form complex fracture networks and provide a highly permeable pathway for fluid transportation. The complex fracture network formed through hydraulic fracturing is named stimulated reservoir volume (SRV), which contributes to shale gas production (Mayerhofer et al., 2010).

To accurately estimate SRV and figure out the key factors that impact the size of SRV is nontrivial. Currently available methods to estimate SRV include microseismic monitoring, tiltmeter measurement, electromagnetic imaging and numerical models. Microseismic monitoring records real-time seismic signals and estimate the approximate range of three-dimensional (3D) SRV from the microseismicity map (Warpinski et al., 2001; Maxwell et al., 2002; Fisher et al., 2004; Maxwell et al., 2009; Warpinski et al., 2009; Zhang et al., 2019; Liu et al., 2021). Microseismic events are created mainly by shear slippages of natural fractures around hydrofractures (Albright et al., 1982; Warpinski et al., 2001; Rutledge and Phillips, 2003). The enhanced pore pressure can reduce the effective stress and cause the critically oriented fractures to become critically stressed and slide. Tiltmeter measurement (Astakhov et al., 2012) uses a surface tiltmeter array to measure the micro-deformation of the surface, which can only provide a much coarser resolution compared with microseismicity maps. The electromagnetic imaging method monitors hydraulic fractures in reservoirs by identifying the contrasts between the electromagnetic properties of the injected proppants and the subsurface (LaBrecque et al., 2016). Nowadays, this method is at the initial state in lab experiments without field applications. Numerical models usually simulate the multi-stage multi-cluster fracturing process coupling the hydrofracture propagation, fluid flow, and the activation of natural fractures (Ren et al., 2016; Wu and Olson, 2016). Significant simplifications of the hydraulic fracturing process and geological structures must be made in numerical models to make the simulation computationally solvable. Therefore, the complexity of natural fracture networks is usually essentially relaxed.

The stimulated reservoir volume is mainly composed of two types of fractures activated in the hydraulic fracturing operation. One type is tensile fractures caused by elevated pore pressure, higher than the minimum principal stress. The

other type is shear fractures attributed to shear slippage, where the elevated pore pressure does not exceed the minimum principal stress but is still large enough to cause the shear failure of preexisting fractures (Maulianda et al., 2014; Wu et al., 2019). Activated natural fractures (both tensile and shear failed fractures) serve as the high-permeable pathway for the fluid pressure propagation. Therefore, preexisting natural fractures are essential for the formation of SRV.

The geometrical and mechanical properties of natural fractures can impact the size of SRV significantly. However, such investigations are rarely conducted. One important reason is that with current technologies, such as borehole images (Prioul and Jocker, 2009), outcrop observations (Abouelresh and Babalola, 2020), 3D seismic techniques (Rijks and Jauffred, 1991) , crosswell imaging techniques (Wilt et al., 1995; Ellefsen et al., 2002), it is almost impossible to have a comprehensive mapping of natural fractures in the subsurface. Therefore, a detailed configuration of SRV is also unavailable. Furthermore, fractures are usually partially sealed instead of being completely sealed. The complex process of crystal growth can result in different sealing patterns, such as massive sealing deposits, thin rinds or veneers that line the surfaces of open fractures, and bridge structures that span otherwise open fractures (Laubach et al., 2004; Lander and Laubach, 2015). The impacts of partially open fractures have rarely been considered in the formation of SRV due to the large scale difference between the fracture sealing and fracture networks (Zhu et al., 2021a). A few preliminary works use the discrete fracture network method to mimic the fracture sealing and the Coulomb failure criterion to distinguish the critical and non-critical stressed fractures (Zhu et al., 2021a,b). They find that partially open fractures can significantly enlarge the size of SRV by connecting more critically orientated fractures. In this research, we further extend the study in Zhu et al. (2021b) and aim to investigate the impact of different fracture properties, including ge-

ometrical properties, mechanical properties and fracture sealing properties, on the formation and development of SRV.

We adopt the stochastic discrete fracture network (SDFN) model method (Lei et al., 2017) to mimic natural fracture networks in the subsurface. By implementing the JRC-JCS model proposed by Barton (1973), we can identify the critically stressed fractures under a given global stress state. This work focuses more on shear fractures and only considers one large tensile hydrofracture caused by hydraulic fracturing. In reality, there might be several tensile fractures in one hydraulic fracturing cluster (Marder et al., 2015; Raterman et al., 2018), but it is usually hard to predict.

We adopt the JRC-JCS model instead of the commonly used Coulomb failure criterion (COULOMB, 1773) because for planar discontinuity surfaces, like a sawn or ground surface, Coulomb failure criterion is a good option to represent the relationship between the peak shear strength τ_p and the normal stress σ_n (Barton et al., 1995; Im et al., 2018; Mattila and Follin, 2019). However, a natural fracture surface in rocks can never be smooth but rough. The undulations and asperities on a natural fracture surface can significantly impact the shear behavior of fractures. In general, a rough surface increases the shear strength and make it more difficult to have shear failures. Barton (1973) proposed an empirical relationship to model the shear strength of rock discontinuities (Barton, 1973; Barton and Choubey, 1977).

$$\tau_p = (\sigma_n - P_p)tan(\phi_r + JRClog_{10}(\frac{JCS}{\sigma_n})), \tag{1}$$

where ϕ_r is the residual friction angle; JRC is the joint roughness coefficient; JCS is the joint wall compressive strength; JRC varies between 0-20, where 0 refers to perfectly smooth surface and 20 is the roughest possible joint without actual steps. If fractures have not been weathered, i.e. fresh fracture,

JCS equals the uniaxial compressive strength of rocks and this value decreases with increasing weathering grades. To determine the proper values for parameters in Eq.1 is nontrivial, which depends on many factors, such as rock types, weathering grades, scales, cementations (Barton and Bandis, 1990; Marinos et al., 2005). Furthermore, Eq. 1 ceases to have any practical meaning for $(\phi_r + JRClog_{10}(\frac{JCS}{\sigma_n}) > 70^\circ$ (Marinos et al., 2005).

Fracture properties considered in this work include three geometries properties (fracture lengths, orientations and positions of fracture centers), two factors related to fracture sealing (the probability of open fractures and the segment length), two mechanical properties (fracture roughness and fracture compressive strength) and one factor of relative fracture intensity. Each factor is represented by a key parameter in the corresponding distribution or definition. Details of each factor are introduced in the next section. In total, eight factors that may impact the formation and development of SRV are considered, and factors are assumed to be independent of each other. A surrogate model is obtained by fitting results of 50,000 realizations, and then a global sensitivity analysis with the Sobol method is conducted. Local stress perturbations induced by interactions of neighbouring fractures are neglected mainly because numerical calculations of stress fields are expensive in complex discrete fracture networks with thousands of realizations. In addition, fractures usually need to be close enough to have a significant stress perturbation (Thomas et al., 2017).

The remainder of this paper is organized as follows: Section. 2 introduces the techniques to construct a typical 2D and 3D fracture networks to mimic subsurface formations. The identification of SRV through incorporating the JRC-JCS failure criterion. The method of sensitivity analysis is introduced as well. Sections. 3 presents results of Sobol sensitivity analysis of each factor on the formation and development of SRV. Section. 4 discusses the insights of

the work on fluid transportation. Important conclusions are summarized in Section. 5.

2. Materials and Methods

This section introduces the construction of a typical two/three-dimensional subsurface formation and the procedures to identify stimulated reservoir volumes. The Sobol method for global sensitivity analysis is introduced.

2.1. 2D/3D stochastic discrete fracture networks

The detailed mappings of fracture networks in the subsurface are usually unavailable with current technologies, such as outcrop observations, wellbore imaging, and 3D seismic mappings. A stochastic discrete fracture network model is a practical method to mimic the natural fracture networks with simplified geometries but preserve essential topological relationships. In this research, a 2D fracture is represented by a line segment, and a square plate represents a 3D fracture for simplicity. As Jing and Stephansson (2007) pointed out, the significance of the fracture shape decreases with an increase in the fracture population size. A square plate is convenient to mimic fracture sealing introduced later.

Three main geometrical properties of fractures are considered, including fracture lengths (2D)/ sizes (3D), orientations, positions of fracture centers. Each geometrical property is described with a widely used statistical distribution (Bonnet et al., 2001). A power-law distribution is implemented to describe fracture lengths,

$$n(l) = \alpha l^{-a}, \tag{2}$$

where $n(l)dl$ is the number of fractures with lengths ranging from $[l, l+dl]$, α is the proportionality coefficient and a is the power-law exponent. The minimum and maximum fracture length used in the power-law distribution is 1 m and

100,000 m. In 3D fracture networks, we generate a unit square with its side length equal to 1 m, then perform the scaling operation on the square with a scale factor of l to change their sizes. Through a simplistic fractal model, we have derived that the power-law exponent has to be larger than one (Zhu et al., 2021c). For most cases, the exponent ranges between 2 and 3 (Bour and Davy, 1997; Bonnet et al., 2001).

The fracture orientations follow von Mises–Fisher distributions (Kemeny and Post, 2003; Whitaker and Engelder, 2005)

$$f(\vec{x}, \vec{\mu}, \kappa) = C(\kappa) \exp(\kappa \vec{\mu}^T \vec{x}), \tag{3}$$

where $C(\kappa)$ is the normalization constant. $\vec{\mu}$ and κ are the mean direction and concentration parameter, respectively. The parameter κ controls the concentration degree of the distribution around the mean direction $\vec{\mu}$. When $\kappa = 0$, the von Mises–Fisher distribution degenerates to a uniform distribution. When κ is large, the distribution is approximate to a normal distribution and concentrates around the angle $\vec{\mu}$ with $1/\kappa$ analogous to σ^2. In this research, we choose $\vec{\mu} = [1, 0]$ for 2D fracture networks and $\vec{\mu} = [1, 0, 0]$ for 3D fracture networks. From a collection of natural outcrop maps (Zhu et al., 2021c), 2D fracture networks usually have their orientations scattered and the corresponding κ is smaller than 3. In this work, we consider a wider range of κ from 0 to 20.

The positions of fracture centers are sampled from a uniform or fractal spatial density distribution. The fractal spatial density distribution (Meakin, 1991; Darcel et al., 2003) introduces clustering effects in the network, which is characterized by a fractal dimension F_D. Real fracture networks are usually clustered, and a fractal spatial density distribution can better describe it (Darcel et al., 2003; Zhu et al., 2021c). For 2D fracture networks, the fractal dimension F_D

varies between 1.1 and 2.0. For 3D fracture networks, the corresponding fractal dimension varies between 2.1 and 3.0.

It is difficult to estimate the fracture intensity in the subsurface from available 1D or 2D measurements (Dershowitz, 1984). However, real subsurface fracture networks should have a much higher fracture intensity than the intensity at percolation if their outcrop maps show good geometrical connectivity. In reality, most outcrop maps are well connected (Zhu et al., 2021c,f). Therefore, we check the cluster in this research and take the fracture intensity at the percolation (formation of a spanning cluster) as the reference. We considered different fracture intensities and described them by a ratio between the number of fractures at termination and the number of fractures at percolation. This ratio is denoted as FI for 2D and 3D fracture networks and varies between 0.8 and 2.6. Therefore, the fracture intensity is larger than the fracture intensity at percolation, and good global connectivity is reached in most cases.

Fig. 1 shows the examples of generated 2D and 3D fracture networks. The fracture networks are generated with an in-house built, open-source software, HatchFrac (Zhu et al., 2021d).

2.2. Identification of stimulated reservoir volume

Without losing generality, we assume a stable strike-slip stress state ($Sh_{min} < S_v < Sh_{max}$). Similar analysis can be extended to a normal or reverse stress state. The injected fluid pressure of hydraulic fracturing is set as the reference stress, i.e. $P_f = 1$. The other important stresses are: the maximum horizontal stress $Sh_{max} = 1.3P_f$, the minimum horizontal stress $Sh_{min} = 0.8P_f$, the vertical stress $S_v = 1.1P_f$; the reservoir pressure is uniformly distributed in considered domain with $P_p = 0.5P_f$. In this work, we only consider one primary hydrofracture in one hydraulic fracturing cluster (Green line segment and square in Fig. 1). The elevated pore pressure caused by hydraulic fracturing is

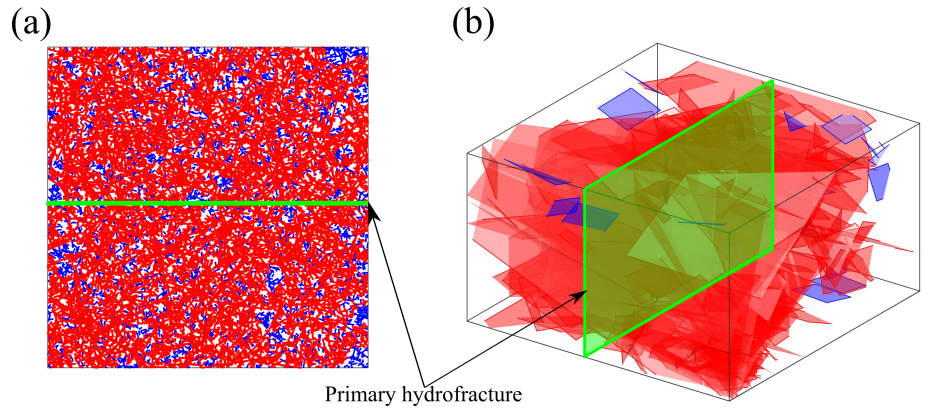

Figure 1: Examples of 2D and 3D fracture networks. For the 2D fracture network (left), the red line segments form the connected spanning cluster. The blue line segments correspond to all other locally connected clusters. The green line segment represents the primary hydrofracture. The fracture orientations follow a uniform distribution ($\kappa = 0$), lengths obey a power-law distribution ($a = 3.0$), positions of fracture centers are uniformly distributed ($F_D = 2.0$). The relative ratio of fracture intensity is 2.0. For the 3D fracture network (right), the red polygons form the connected spanning cluster. The blue squares correspond to all other locally connected clusters. The green square represents the primary hydrofracture. The fracture orientations follow a uniform distribution ($\kappa = 0$), lengths obey a power-law distribution ($a = 3.0$), positions of fracture centers follow a fractal spatial density distribution ($F_D = 2.5$). The system size is 100 for the 2D fracture network and 10 for the 3D fracture network to have a better visualization. The relative ratio of fracture intensity is 1.5.

assumed to be constant along the hydraulic fracture and decreases linearly with increasing distance. Stress states are critical for the formation of SRV, but they are strongly case-dependent and here we only analyze a typical scenario.

JRC-JCS failure criterion (Eq. 1) is implemented to identify critically/non-critically stressed fractures, where the residual friction angle ϕ_r is set as 30 degrees. JRC varies between 0 (perfectly smooth) and 20 (roughest). JCS varies between $0.5P_f$ and 18.5 P_f.

Fracture sealing is simulated by dividing 2D fractures into small segments. Each small segment can be sealed and can block the flow of the fluid. The degree of fracture sealing is controlled by two parameters, the probability of open fractures (P_o) and the segment length (L_{se}). The segment length is the minimum unit of fracture sealing, which can reach a millimeter in reality, but is impractical in the numerical simulation because of the limited computation

capacity. Therefore, we choose decreasing segment lengths from 1 m to 0.2 m to show the impact of the segment length. 3D fractures are divided into small grids to mimic the fracture sealing. Detailed introduction of this method can be found in (Zhu et al., 2021a,b). The probability of open fractures is defined as:

$$P_o = \frac{L_{open}}{L_{total}}, \tag{4}$$

where L_{open} is the total length of open fractures and L_{total} is the total length of all fractures. In a 3D fracture network, the fracture length is replaced with the fracture area.

In this research, we consider a 100 $m \times 100$ m square domain for 2D formations and a 50 $m \times 50$ $m \times 50$ m cubic system for 3D formations. From microseismicity observations, the SRV usually shows an elongated shape in most cases (Shaffner et al., 2011; Raterman et al., 2018). Therefore, we assume the farthest distance where the injected fluid pressure can propagate is 20% of the system size on each side of the hydrofracture.

After generating discrete fracture networks, we can identify stimulated reservoir volume (SRV) based on the given stress state and JRC-JCS criterion. The SRV comprises two main parts: one is the critically stressed fractures, and the other is the partially open fractures. Critically stressed fractures form the backbone of SRV, while partially open fractures can further enlarge SRV. Fig. 2(a) shows the SRV composed of critically stressed fractures. Red fractures are critically stressed fractures, and they are connected to the primary hydrofracture directly or indirectly. Therefore, the elevated pore pressure in the hydrofracture can propagate to those fractures. The purple fractures are critically orientated fractures because they are not connected to the primary hydrofracture, and the high fluid pressure cannot be transmitted to purple fractures. Fig. 2(c) shows the SRV composed of both critically stressed fractures and partially fractures.

Partially open fractures have enlarged the SRV by connecting more critically orientated fractures to the hydrofracture and making them critically stressed. The total lengths of permeable fractures in Figs. 2(a) and (c) are denoted as L_{cs} and L_{cso} , respectively. L_{cs} is 2026 m, and L_{cso} is 5078 m. Fig. 2(b) show the SRV composed of critically stressed fractures in 3D. Fig. 2(d) show the SRV composed of critically stressed fractures plus partially open fractures. The total areas of permeable fractures (red fractures) in Figs. 2(b) and (d) are denoted as A_{cs} and A_{cso}. The system size is 10 m in Figs. 2 (b) and (d) for demonstration because it is difficult to visualize a 3D fracture network with thousands of fractures in a large system. A_{cs} is 513 m^2, and A_{cso} is 1810 m^2. In linear flow, the flux from the matrix to fractures is proportional to the fracture area (Bello et al., 2010; Haider et al., 2020), suggesting that partially sealed fractures can increase reservoir production by enlarging the stimulated reservoir volume.

In this research, we demonstrate the contribution of partially open fractures by performing a full-scale, embedded discrete fracture network model simulation with UNCONG software (Li et al., 2015). For simplicity, all critically stressed fractures and partially open fractures are assigned with a permeability of 10 darcies, and sealed fractures are impermeable. The matrix has a low permeability of 0.05 micro darcies. The primary hydrofracture is replaced with a horizontal production well to implement boundary conditions and schedule control conveniently. The initial reservoir pressure is set as 300 bar, and the bottomhole pressure is set as 100 bar and kept constant. We simulate the production for ten days and compare the production difference with and without partially open fractures. Detailed input parameters are listed in Table. 1. Fig. 3(a) shows changes of the gas formation volume factor and gas viscosity with pressure. Figs. 3 (b) and (c) show the relative permeability curves in the matrix and fractures, respectively.

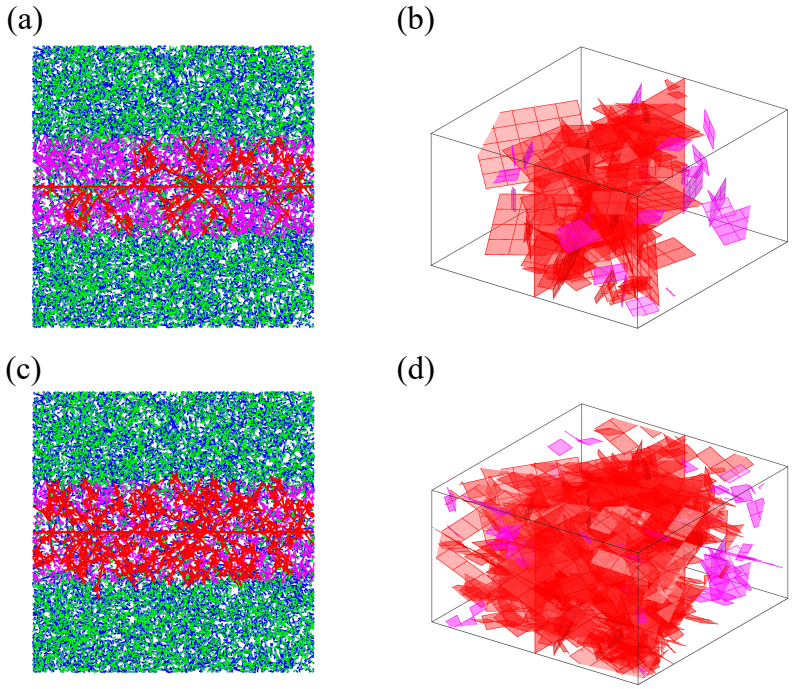

Figure 2: Demostration of 2D/3D SRV composed of only critically stressed fractures (a,b) or critically stressed fractures plus partially open fractures (c,d). The probability of open fractures is 0.5 for both 2D and 3D fracture networks. The fracture surface is assumed to be smooth ($JRC = 0$). In 2D fracture networks (a,c), the red line segments form the SRV. The purple fractures are critically orientated fractures. The green line segments are open fractures, and the blue line segments are sealed fractures. In 3D fracture networks (b, d), open and sealed fractures are not shown for better visualization. The red squares form the SRV, and the purple squares are critically orientated fractures.

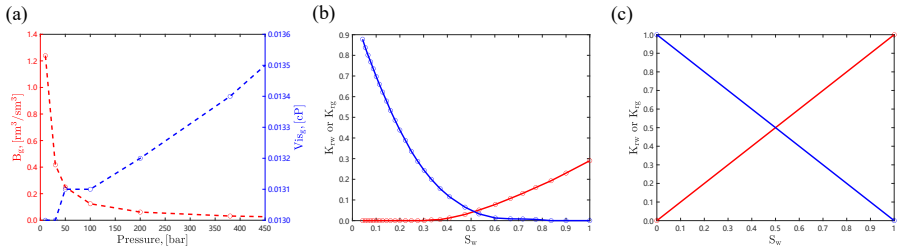

Figure 3: (a) Changes of the formation gas volume factor (B_g) and gas viscosity (Vis_g) with pressure; (b) The relative permeability curve in the matrix; (c) The relative permeability curve in fractures

Figs. 4 (a) and (b) show the pressure distribution of two scenarios after ten days of production, where one only consider the critically stressed fractures

Table 1: Input parameters for the simulation

Matrix permeability, k_m, [μd]	0.05
Matrix porosity	0.05
Fracture permeability, k_f, [d]	10
Fracture porosity	1.0
The coefficient of water compressibility, [bar^{-1}]	3.15e-6
The coefficient of water viscosity compressibility, [cP $\cdot$ bar^{-1}]	2.10e-6
Initial water satuation	0.5
Initial reservoir pressure, P_i, [bar]	300
Constant bottomhole pressure, [bar],	100

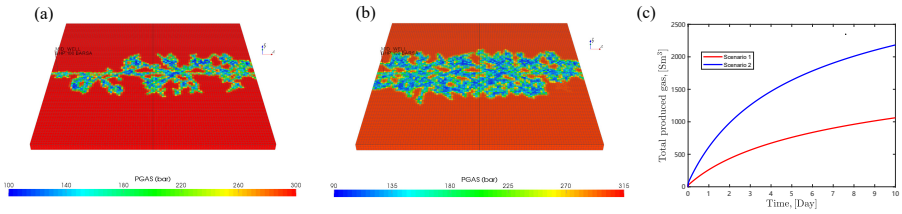

Figure 4: (a) Pressure distribution in Scenario 1, where the SRV comprises critically stressed fractures only. (b) Pressure distribution in Scenario 2, where the SRV comprises critically stressed plus partially open fractures. (c) The comparison of the total production of gas in two scenarios

and the other one consider both critically stressed and partially open fractures. Figs. 4 (c) shows the comparison of the total production of gas in these two scenarios. The simplified simulation is different from an actual production case. However, it straightforwardly demonstrates the significant contribution of partially open fractures by connecting more critically orientated fractures and enlarging the size of SRV. The total length in the first scenario is 2026 m, while this value is 5078 m in the second scenario. The ratio of the total fracture length between the two scenarios is 2.51, and the ratio of the total production of gas in the two scenarios is 2.05. Therefore, the shale gas production is proportional to the fracture length in the connected cluster. In 3D, the production is proportional to the total fracture area.

In the following sections, we will systematically analyze the impact of each fracture property by implementing the global sensitivity analysis. The factors

include three geometrical properties (the exponent of the power-law distribution (a), the fractal dimension of the fractal spatial density distribution (F_D), the concentration parameter in a von Mises–Fisher distribution (κ)), two factors related to the fracture sealing (the probability of open fractures (P_o) and the segment length (L_{se})), two factors related to the mechanical properties of fracture surfaces (joint roughness coefficient (JRC) and joint wall compressive strength (JCS)) and one relative fracture intensity (FI). In 2D fracture networks, three essential parameters are selected as the response parameters: the total length of connected critically stressed fractures, L_{cs}, the total length of connected critically stressed fractures plus partially open fractures, L_{cso}, and the relative increase of fracture length, RI_{2D}. For 3D fracture networks, the fracture area replaces the fracture length, and the corresponding response parameters are A_{cs}, A_{cso} and RI_{3D}.

The relative increase is defined in Eq. 5, which represents the contribution of partially open fracture on enlarging the size of SRV.

$$RI_{2D} = \frac{L_{cso} - L_{cs}}{L_{cs}} \tag{5}$$

In 3D fracture networks, a similar formula is applied with the fracture length replaced with the fracture area. A detailed summary of factors and responses are listed in Tables. 2 and 3. Five hundred cases with each factor randomly chosen from the given interval (Table. 2) are simulated for the following sensitivity analysis. For each considered case, the results are averaged over 100 random realizations for stabilization.

2.3. Global sensitivity analysis

This research evaluates the impact of each factor and their interactions with the Sobol' indices (IM, 1993). To simplify the notation without losing generality,

Table 2: Factors in the global sensitivity analysis

Factor	Range	Property	Definition
a	$[2, 3]^{2/3D}$	Fracture length	The exponent of a power-law distribution
F_D	$[1.1, 2]^{2D}$, $[2.1, 3]^{3D}$	Position of fracture centers	The fractal dimension of a fractal spatial density distribution
κ	$[0, 20]^{2/3D}$	Fracture orientation	The concentration parameter in a von Mises–Fisher distribution
FI	$[0.8, 2.6]^{2/3D}$	Fracture intensity	The ratio between the number of fractures at termination and at percolation
P_o	$[0.2, 0.8]^{2/3D}$	Fracture sealing	The ratio of the total length/area of open fractures and total fractures
L_{se}	$[0.2\text{ m}, 1\text{ m}]^{2D}$, 1 m^{3D}	Fracture sealing	The minimum unit of fracture sealing
JRC	$[0, 20]^{2/3D}$	Fracture roughness	Joint roughness coefficient in the JRC-JCS model
JCS	$[0.5, 18.5]P_f^{2/3D}$	Fracture strength	Joint wall compressive strength in the JRC-JCS model

Note: superscripts, $2D$, $3D$ and $2/3D$, refer to 2D fracture networks, 3D fracture networks, and both 2D and 3D fracture networks.

Table 3: Responses in the global sensitivity analysis

Response	Dimension	Definition
L_{cs}	2D	The total length of critically stressed fractures
L_{cso}	2D	The total length of critically stressed plus partially open fractures
RI_{2D}	2D	Ratio between $(L_{cso} - L_{cs})$ and L_{cs}
A_{cs}	3D	The total area of critically stressed fractures
A_{cso}	3D	The total area of critically stressed plus partially open fractures
RI_{3D}	3D	Ratio between $(A_{cso} - A_{cs})$ and A_{cs}

we assume the input variables are uniformly distributed in [0,1]. Therefore, the support of the input set with n variables is a n-dimensional unit hypercube $\mathcal{S} = [0,1]^n$. The Sobol method is a variance-based method, which represents a deterministic model, $Y = f(\mathbf{X})$, as a sum of elementary functions:

$$f(x_1, x_2, \ldots, x_n) = f_0 + \sum_{i=1}^{n} f_i(x_i) + \sum_{1 \le i < j < n} f_{ij}(x_i, x_j) + \cdots + f_{1,2,\ldots,n(x_i,x_2,\ldots,x_n)} \tag{6}$$

This expansion is unique under conditions:

$$\int_0^1 f_{i_1 \ldots i_s} dx_{i_k} = 0,\ 1 \le k \le s,\ \{i_1, \ldots, i_s\} \subseteq \{1, \ldots, d\}, \tag{7}$$

This means f_0 is constant, which equals to the expected value of $f(\mathbf{X})$. $\mathbf{X}$ is the input vector composed of n random variables ($\mathbf{X} = \{x_1, x_2, \ldots, x_n\}$), which are mutually independent.

Analogously, the model's total variance can be decomposed as the sum of the variances of the summands.

$$Var(Y) = \sum_{i=1}^{n} D_i(Y) + \sum_{1 \le i < j < n} D_{ij}(Y) + \cdots + D_{1,2,\ldots,n}(Y), \tag{8}$$

where $D_i(Y) = Var[\mathbb{E}(Y \mid x_i)]$, $D_{ij}(Y) = Var[\mathbb{E}(Y \mid x_i, x_j)] - D_i(Y) - D_j(Y)$ and so on for higher order interactions. The decomposition of the variance leads to the Sobol' indices as follows, which can be adopted as a sensitivity measure.

$$S_i = \frac{D_i(Y)}{Var(Y)},\ S_{ij} = \frac{D_{ij}(Y)}{Var(Y)},\ \ldots \tag{9}$$

The Sobol' indices represent the relative contribution of each factor or their combinations. The index concerning individual factor x_i is called the first-order Sobol' index (S_i). Multiple-term indices, e.g. $S_{ij},\ i \neq j$, are referred to as higher-order Sobol' indices (interaction indices), which account for the effects

of interactions of the factor pair x_i and x_j.

The total Sobol' index of input factor x_i, denoted S_i^T, is the sum of all the Sobol' indices involving this factor:

$$S_i^T = S_i + \sum_{i \neq j} S_{ij} + \sum_{j \neq i, k \neq i, j<k} S_{ijk} + \cdots = \sum_{l \in \#i} S_l \tag{10}$$

where $\#i$ are all the subsets of $\{1, \ldots, n\}$ including i. In practice, when n is large, only the total Sobol' indices (total effects), the first-order Sobol' indices (the main effects) and the second-order Sobol indices (the interaction effects) are computed.

In this work, we use a surrogate model to represent the deterministic model described in Section 2.2. The surrogate model is a third-order polynomial function obtained through an ordinary least squares regression with 500 cases. After obtaining the surrogate model, 250,000 samples are collected with a Latin hypercube sampling method to evaluate the global sensitivity of the response concerning each factor and interactions between factors. The analysis is conducted with a open-source MATLAB software, UQLAB (Marelli and Sudret, 2014).

3. Results

This section analyses the impact of each factor and interactions between different factors on the formation and development of SRV. The formation and development of SRV is represented by three response parameters (L_{cs}, L_{cso} and RI_{2D} in 2D fracture networks and A_{cs}, A_{cso} and RI_{3D} in 3D fracture networks). The sensitivity analysis with each factor as the response is conducted separately.

3.1. Sensitivity analysis in 2D fracture networks

The variations of L_{cs}, L_{cso} and RI_{2D} in 500 cases are shown in Figs. 5 and 6. In Fig. 5, L_{cs} and the corresponding L_{cso} are linked with a line segment to

demonstrate the difference between these two values in each case. The mean value of L_{cs} and L_{cso} are 398.3 m and 1762.5 m. Therefore, it is obvious that partially open fractures can enlarge the size of SRV and contribute to production. The mean value of the relative increase of SRV is about 4. However, the mean value can be sensitive to extreme values. A median value may be closer to reality, which is 0.42 in 500 cases.

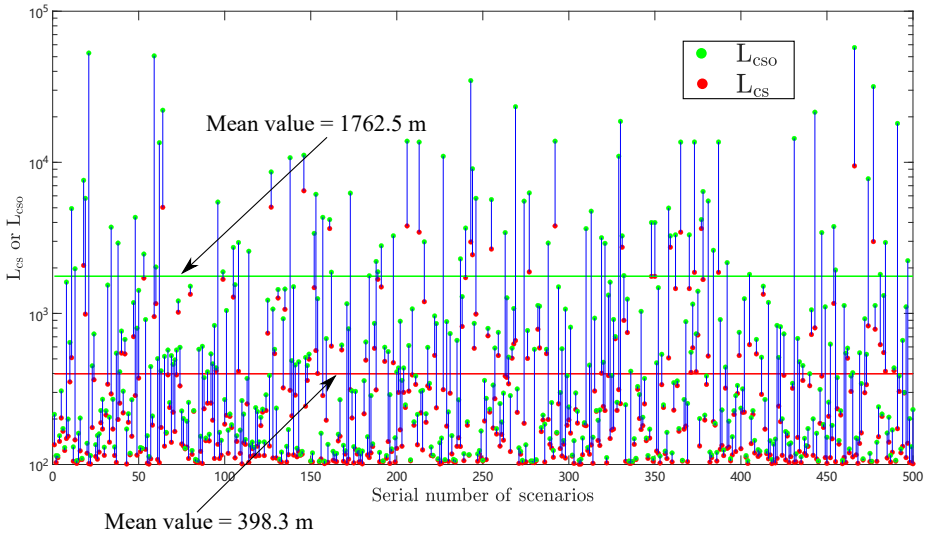

Figure 5: L_{cs} and L_{cso} variations in 500 scenarios

Fig. 7 shows results of the global sensitivity analysis with the total length of critically stressed fractures (L_{cs}) as the response. Fig. 7(a) shows the goodness of the multivariate polynomial fit, which has an R-square value of 0.95 between the simulation results and predictions. The first order Sobol' indices (Fig. 7(c)) reflect the sensitivity of the individual factor. For the total length of critically stressed fractures, L_{cs}, the fracture roughness (JRC), the exponent of the power-law distribution (a) and the concentration parameter in the von Mises–Fisher distribution (κ) are the most influential factors. The fracture sealing factors (P_o and L_{se}) are irrelevant to L_{cs} because critically stressed fractures only depend on the JRC-JCS model. The fracture sealing can impact

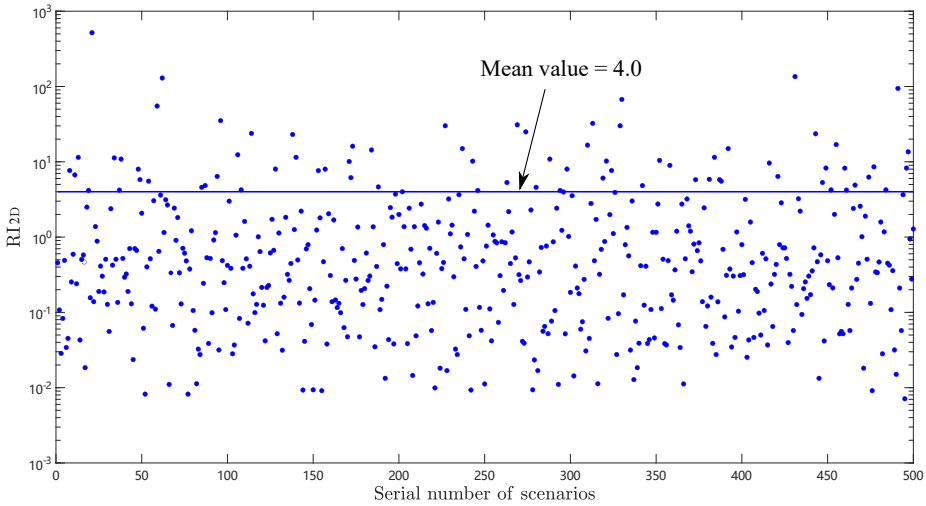

Figure 6: RI_{2D} variations in 500 scenarios

the shear slippage if it significantly changes rock strength at the failure plane. However, in this research, factors are assumed to be independent of each other. The second-order Sobol' indices show interactions between factors and the top five pairs of factors are shown in Fig. 7(d), including $a - JRC$, $a - \kappa$, $FI - \kappa$, $FI - JRC$ and $a - JCS$. After considering interactions between factors, the total Sobol' indices shows the total effect of each factor in Fig. 7(b). The Sobol' index of each factor has increased due to interactions between factors, but the relative ranking is the same. The fracture roughness has an essential impact on the total length of critically stressed fractures. From correlation analysis, the correlation coefficient between JRC and L_{cs} is -0.34. Therefore, JRC has a negative correlation with L_{sc}. A rougher fracture surface (a larger JRC value) can enlarge the general friction angle as shown in the JRC-JCS model, making the failure harder.

Fig. 8 shows results of the global sensitivity analysis with the total length of critically stressed plus partially open fractures (L_{cso}) as the response. Fig. 8(a) shows the goodness of the multivariate polynomial fit, which has an R-square

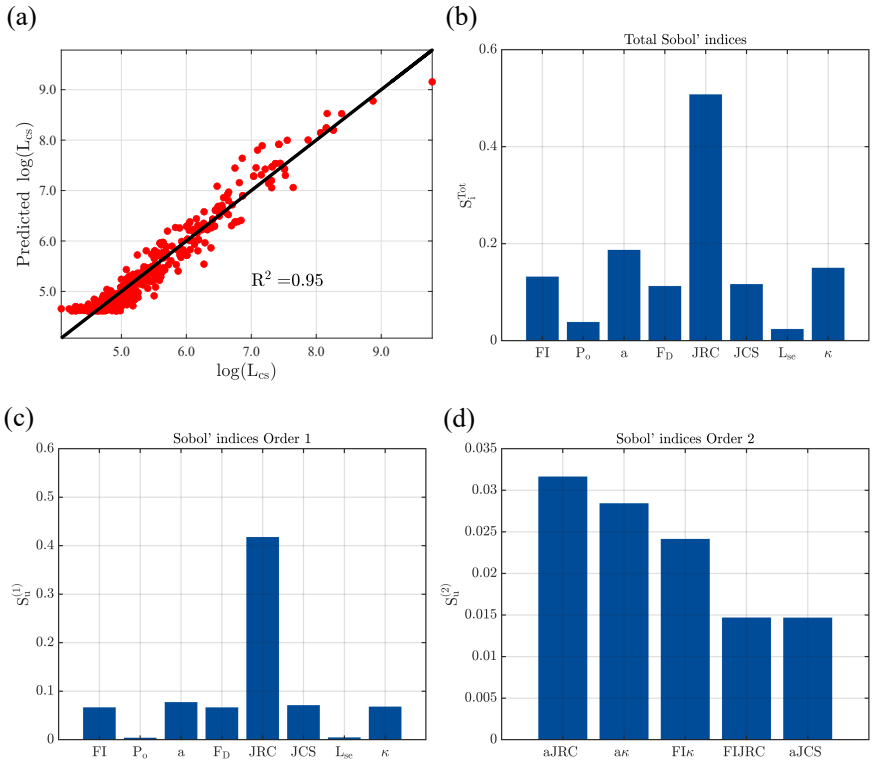

Figure 7: Sensitivity analysis with L_{cs} as the response. (a) The multivariate polynomial fit of L_{cs} in 500 cases. (b) The total Sobol' indices show the total effect of each factor. (c) The first-order Sobol' indices show the main effect of each factor. (d) The second-order Sobol' indices show the interaction effects of factors.

value of 0.95 between the simulation results and predictions. According to the first order Sobol' indices (Fig. 8(c)), the exponent of the power-law distribution (a), the fractal dimension of the fractal spatial density distribution (F_D) and the probability of open fractures (P_o) are the most influential factors. The least influential factors are the concentration parameter (κ), joint compressive strength (JCS), and the segment length (L_{se}). The top five pairs of factors are shown in Fig. 8(d), including $P_o - a$, $a - F_D$, $FI - P_o$, $P_o - L_{se}$ and $FI - a$. After considering the interactions between factors, the total Sobol' indices shows the total effect of each factor in Fig. 8(b). The Sobol' index of each factor has increased due to the interaction between factors, but the relative ranking is

the same. The exponent of the power-law distribution has the essential impact on L_{cso}. A larger exponent means more small fractures dominate the system. From simple correlation analysis, we find the correlation coefficient is 0.34, which means that the exponent has a positive correlation with L_{cso} and more small fractures can make L_{cso} larger.

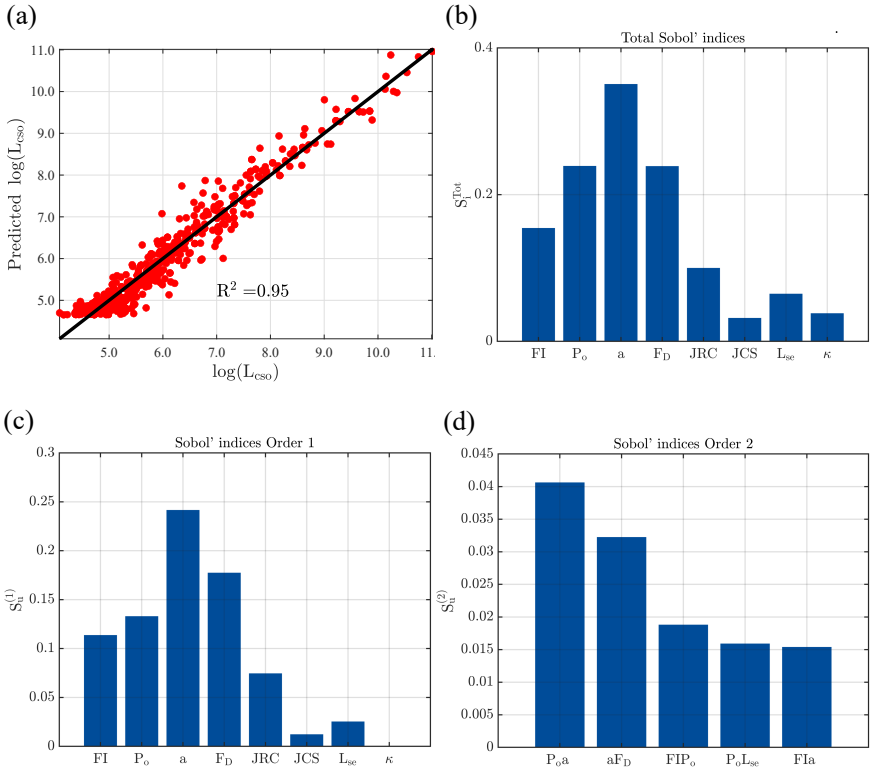

Figure 8: Sensitivity analysis with L_{cso} as the response

Fig. 9 shows results of the global sensitivity analysis with the relative increase of SRV (RI_{2D}) as the response. Fig. 8(a) shows the goodness of the multivariate polynomial fit, which has an R-square value of 0.95 between the simulation results and predictions. Based on the first order Sobol' indices (Fig. 8(c)), the exponent of the power-law distribution (a), the fractal dimension of the fractal spatial density distribution (F_D) and the probability of open fractures (P_o) are

the most influential factors. The least influential factors are the concentration parameter (κ), the joint compressive strength (JCS), and the segment length (L_{se}). The top five pairs of factors are shown in Fig. 8(d), including $P_o - \kappa$, $a - JRC$, $P_o - a$, $a - F_D$ and $P_o - L_{se}$. After considering the interactions between factors, the total Sobol' indices shows the total effect of each factor in Fig. 8(b). Compared with the result in Fig. 8, impacts of each factor on RI_{2D} are almost the same as impacts on L_{cso}. The interactions between factors do not change the sensitivity ranking. The exponent of the power-law distribution has the essential impact on RI_{2D}. The correlation coefficient between a and RI is 0.16, indicating a positive correlation. Therefore, the contribution from partially open fractures is more significant in fracture networks dominated by small fractures.

In summary, mechanical properties, such as fracture roughness (JRC) and fracture strength (JCS), and fracture orientations (κ) are essential to trigger shear slippage of natural fractures and form the backbone of SRV. Partially open fractures can connect more critically orientated fractures and enlarge the size of SRV. After considering partially open fractures, fracture sealing properties and geometrical properties of fractures become essential, such as P_o (the probability of open fractures), a (the fracture length) and F_D (the fracture center positions).

3.2. Sensitivity analysis in 3D fracture networks

In 3D fracture networks, we consider seven factors, excluding the segment length because of the limited computational capacity. In addition, from the analysis in 2D fracture networks, the segment length does not significantly impact the formation and development of SRV.

The variations of A_{cs}, A_{cso} and RI are shown in Figs. 10 and 11. In Fig. 10, A_{cs} and the corresponding A_{cso} are linked with a line segment in each case to show the difference between these two values. Compared with 2D cases,

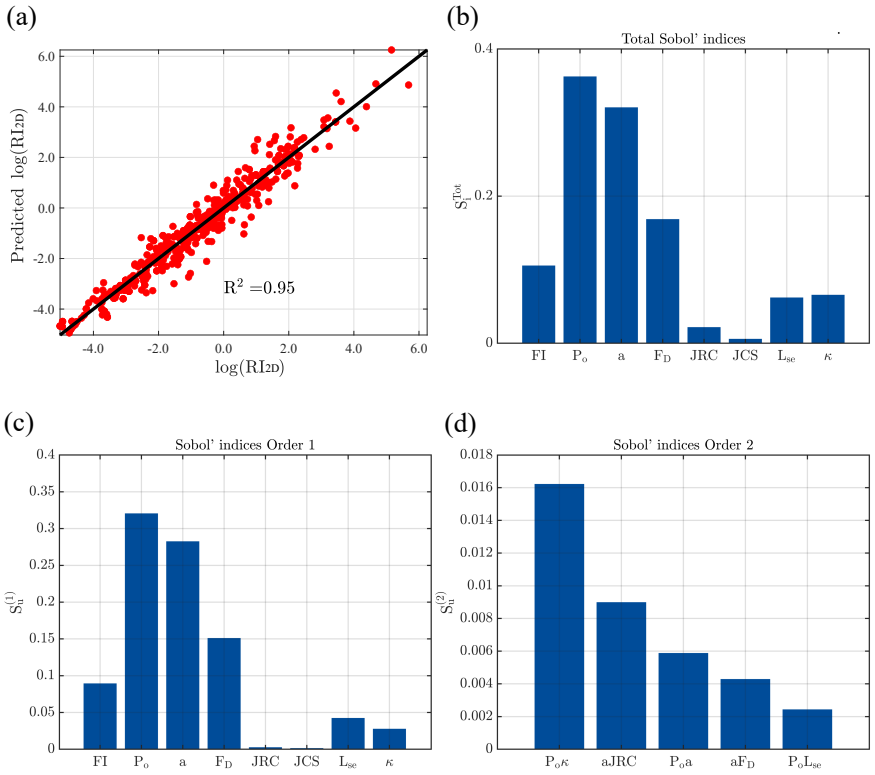

Figure 9: Sensitivity analysis with RI_{2D} as the response

the partially open fractures have more significant enlargement of SRV in 3D fracture networks. The mean value of A_{cs} and A_{cso} are 2962 m^2 and 34688 m^2. Therefore, partially open fractures can significantly enlarge the size of SRV and contribute to production. The mean value of the relative increase of SRV is about 11, and the median value is 8.5 in 500 cases, which are much higher than the values in 2D fracture networks.

Fig. 12 shows results of the global sensitivity analysis with the total area of critically stressed fractures (A_{cs}) as the response. Fig. 12(a) shows the goodness of the multivariate polynomial fit, which has an R-square value of 0.96 between the simulation results and predictions. The first order Sobol' indices (Fig. 12(c)) reflect the sensitivity of individual factors. The most influential factors are

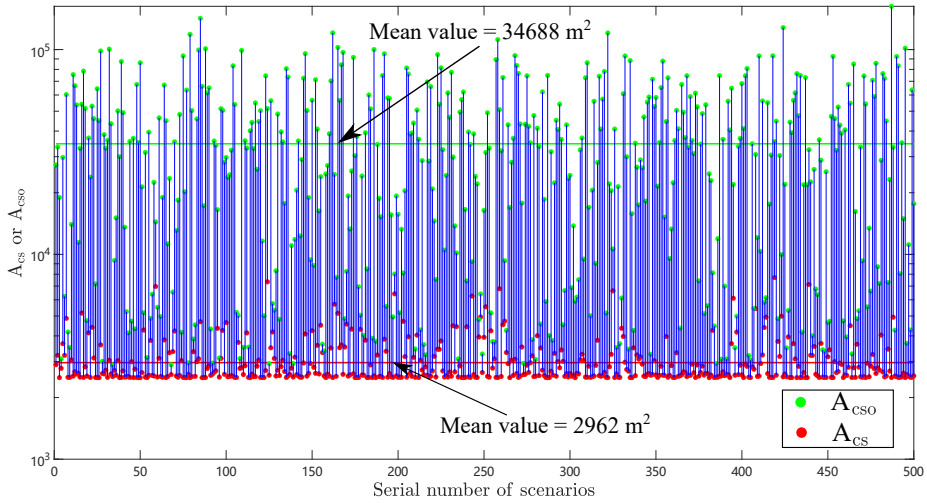

Figure 10: A_{cs} and A_{cso} variations in 500 scenarios

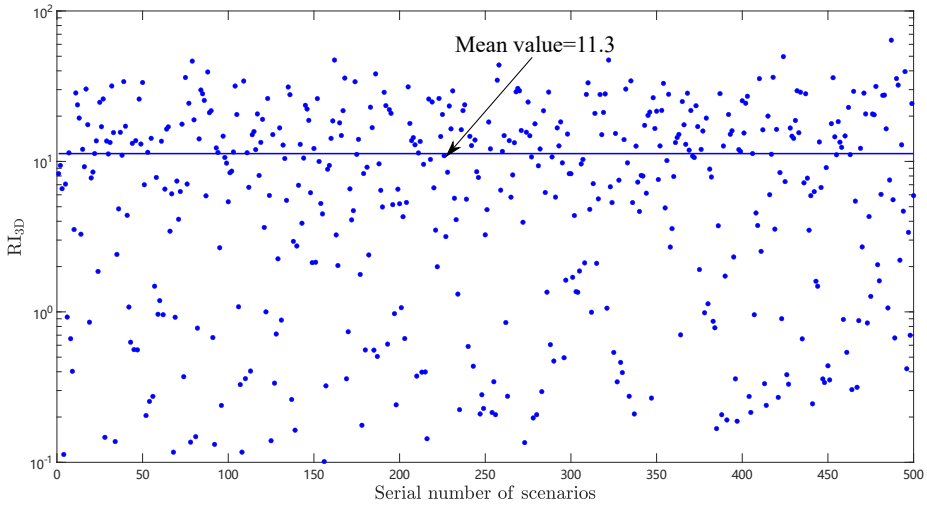

Figure 11: RI_{3D} variations in 500 scenarios

the fracture roughness (JRC), the concentration parameter (κ), and the joint compressive strength (JCS). This observation is similar to the result in 2D fracture networks. The probability of open fractures (P_o) is irrelevant to the critically stressed fractures because the JRC-JCS model completely constrains the critically stressed states. In contrast with 2D fracture networks, fracture

geometrical properties, a and F_D, do not change the response significantly. The second-order Sobol' indices show the interactions between factors, and the top five pairs of factors are shown in Fig. 12(d), including $\kappa - JRC$, $FI - JRC$, $JRC - JCS$, $\kappa - JCS$ and $FI - \kappa$. After considering the interactions between factors, the total Sobol' indices shows the total effect of each factor in Fig. 12(b). The Sobol' index of each factor has increased due to the interaction between factors, but the relative ranking has not changed. The fracture roughness has an essential impact on the total length of critically stressed fractures. From correlation analysis, the correlation coefficient between JRC and A_{cs} is -0.57. Therefore, JRC has a negative correlation with A_{sc}. A rougher fracture surface (a larger JRC value) can enlarge the general friction angle as shown in the JRC-JCS model, making the failure harder.

Fig. 13 shows results of the global sensitivity analysis with the total length of critically stressed fractures plus the partial open fractures (A_{cso}) as the response. Fig. 13(a) shows the goodness of the multivariate polynomial fit, which has an R-square value of 0.98 between the simulation results and predictions. According to the first order Sobol' indices (Fig. 13(c)), the probability of open fractures (P_o), the relative fracture intensity (FI) and the concentration parameter (κ) are the most influential factors. However, P_o is the most dominant factor compared with all other six factors. The top five pairs of factors with interaction effects are shown in Fig. 13(d), including $P_o - \kappa$, $FI - P_o$, $P_o - JRC$, $P_o - a$ and $a - F_D$. After considering the interactions between factors, the total Sobol' indices shows the total effect of each factor in Fig. 13(b). The results are not changed with the first order Sobol' indices. The correlation coefficient between P_o and A_{cso} is 0.73, indicating a strong positive correlation between these two parameters, and more open fractures lead to a larger SRV.

Fig. 14 shows results of the global sensitivity analysis with the relative in-

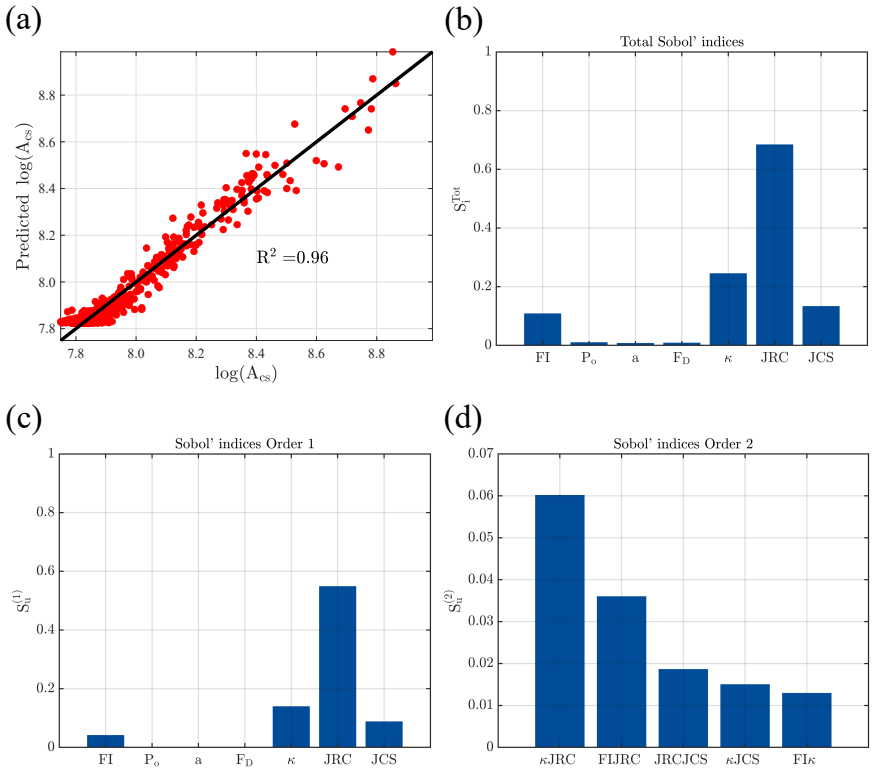

Figure 12: Sensitivity analysis with A_{cs} as the response

crease of SRV (RI_{3D}) as the response. Fig. 14(a) shows the goodness of the multivariate polynomial fit, which has an R-square value of 0.99 between the simulation results and predictions. The results are similar to the results of A_{cso}. The second-order Sobol' indices are small, indicating negligible interactions between factors. The probability of open fractures is the most significant factor in the relative increase of SRV. All other six factors are insignificant. The correlation coefficient between P_o and RI_{3D} is 0.71, indicating a strong positive correlation.

In summary, mechanical properties of fractures, fracture roughness (JRC) and fracture strength (JCS), and fracture orientations (κ) are essential to the formation of critically stressed fractures. Partially open fractures can signifi-

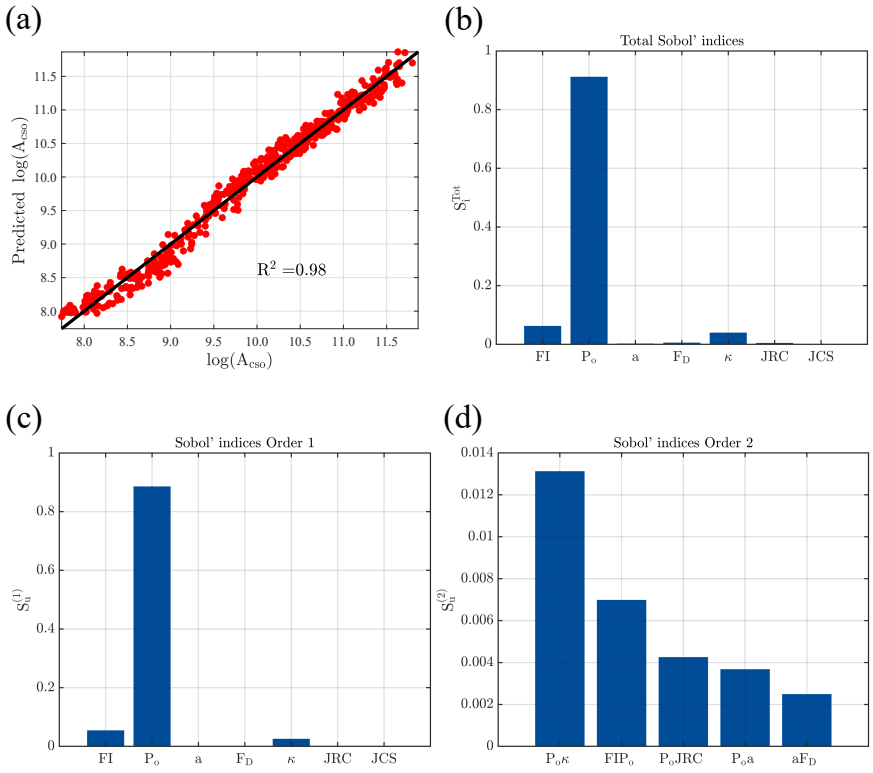

Figure 13: Sensitivity analysis with A_{cso} as the response

cantly enlarge the SRV by connecting more critically orientated fractures. The important factors include the probability of open fractures (P_o), fracture intensity (FI), and fracture orientations (κ). The probability of open fractures (P_o) is the most dominant factor among all six factors. Fracture geometrical properties, fracture length (a), and center positions (F_D) are insignificant for SRV enlargement in 3D fracture networks.

3.3. Comparison of results in 2D and 3D fracture networks

The global sensitivity analysis results are similar for both 2D and 3D fracture networks in terms of the total length (area in 3D) of critically stressed fractures. The fracture roughness (JRC), fracture orientations (κ), fracture

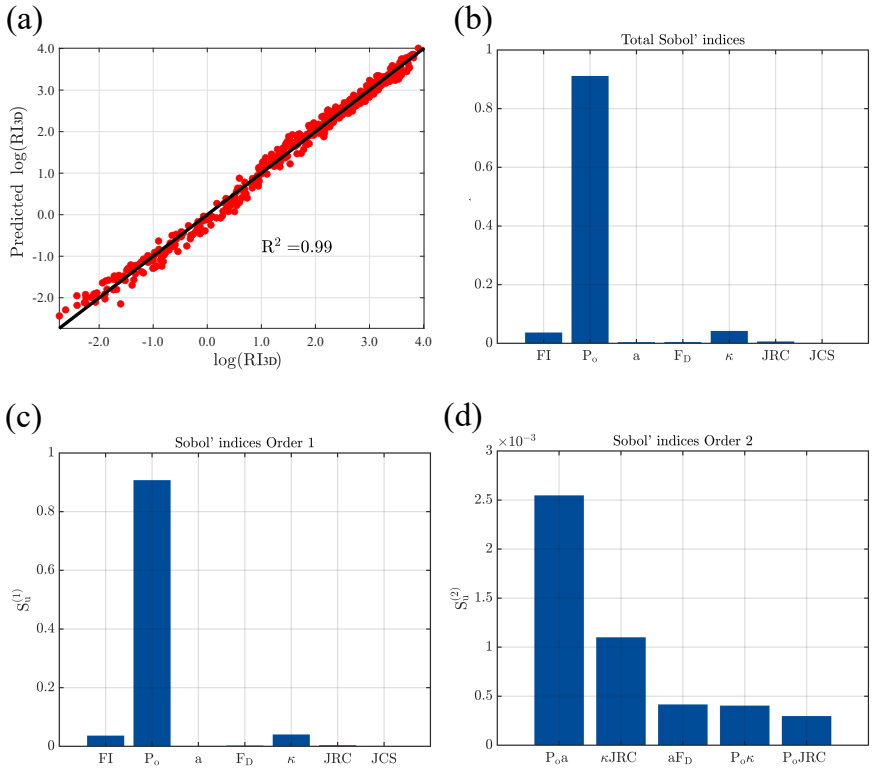

Figure 14: Sensitivity analysis with RI as the response

strength (JCS) are important for the formation of critically stressed fractures. For the contribution of partially open fractures, represented by L_{cso}, A_{cso}, RI_{2D} and RI_{3D}, the probability of open fractures (P_o) are the most significant factor for both 2D and 3D fracture networks. However, important geometrical properties of fractures, i.e. fracture length (a) and fracture center positions (F_D), have significantly different behaviors in 2D and 3D fracture networks. This phenomenon is partially due to the different effects of geometrical properties on the connectivity of 2D and 3D fracture networks.

The connectivity of a fracture network is essential for the formation of SRV. Fracture geometries can impact the connectivity of fracture networks at percolation (Zhu et al., 2021e). Here, the percolation state refers to the formation

of a spanning cluster in the fracture system. This work defines relative fracture intensity as the ratio between the total number of fractures at termination and at percolation. This value varies from 0.8 to 2.6. Therefore, for most cases, the global connectivity of the fracture network is good since a spanning cluster is formed in the system. From our recent analysis of 80 natural outcrop maps (Zhu et al., 2021c,f), we found that 3D subsurface fractures have to be pervasive if their outcrop maps show good geometrical connectivity. Most natural outcrop maps have a spanning cluster formed and show good geometrical connectivity(Zhu et al., 2021c). Therefore, it is close to reality that the real subsurface fracture networks have their RI larger than 1, which means the three-dimensional fracture networks have a much higher fracture intensity than the intensity at percolation. It is also meaningful to discuss SRV when fractures are well-developed because formations with sparse fractures cannot yield good production after the hydraulic fracturing operation.

Clustering effects and small fractures usually have negative impacts on the global connectivity of fracture networks (Zhu et al., 2021e). However, in this work, the correlation coefficients of $a - RI_{2D}$ and $F_D - RI_{2D}$ are 0.16 and -0.07 (slightly negative), which means that small fractures and clustering effects can enlarge the size of SRV. This inconsistency is possibly due to differences between global and local connectivity. For SRV, the local connectivity close to the hydrofracture is more important than the global connectivity of the entire system. For global connectivity, large fractures are essential for long-distance interactions, especially for sparse fracture systems. However, for local connectivity, especially in this work, where most fracture networks have a spanning cluster formed, the impact of large fractures are not significant. Clustering effects cannot contribute much to global connectivity but can enhance local connectivity(Zhu et al., 2018). Therefore, small fractures and clustering effects

are beneficial to the relative increase of SRV (RI_{2D}) in 2D fracture networks.

For 3D fracture networks, both fracture lengths and clustering effects are insignificant for the relative increase of SRV (RI_{3D}). 3D fracture networks are not sensitive to clustering effects as observed in Zhu et al. (2021e). Therefore, their impact on the formation of SRV is also insignificant. Variations of fracture lengths in 3D fracture networks are also negligible but significant in 2D fracture networks. This phenomenon is partially caused by the convenient interactions between three-dimensional fractures because they can intersect the other fractures in a volume, but 2D fractures are constrained in the same plane. For 3D fracture networks with a high fracture intensity, fracture lengths and center positions of the fracture network are not significant to enhance the local connectivity. Instead, the probability of open fractures P_o is significant for SRV development because it determines the hydraulic connectivity of fracture networks. Fracture orientations are also crucial because they affect the mechanical response of natural fractures.

4. Discussions on the fluid transportation

For formations with ultra-low permeabaility, such as shale gas reservoirs or enhanced geothermal systems, the hydraulic fracturing operation is necessary to extract fluid economically. Hydrofractures and stimulated natural fractures (SRV) provide the main permeable pathway for fluid flow. Real fractures are complex in terms of their irregular shapes, complex rough surfaces, the tortuosity of flow paths in fractures and stress impacts on the hydraulic apertures. However, among all complexities, the configuration of SRV has the most significant impact on fluid transportation because it quantifies the connected permeable fractures. However, the detailed configuration of SRV is unavailable with current technologies. The commonly adopted idealized configuration of

SRV is an orthogonal fracture network around the hydraulic fractures (Fisher et al., 2002, 2004). This configuration is not physically meaningful for most stress states because natural fractures perpendicular to hydraulic fractures are parallel to the minimum principal stress. Substantial fluid pressure is required to overcome the maximum principal stress and make those natural fractures critically stressed. In reality, it is almost impossible to reach such a significant condition of fluid pressure.

This work provides a preliminary framework for identifying SRV configurations by constructing subsurface formations with stochastic discrete fracture networks and implementing the JRC-JCS failure criterion. Although actual subsurface structures are largely unknown, two aspects of efforts can be emphasized to make the model more realistic and trustworthy. One is to constrain the discrete fracture network model with more available data, including geological and geomechanical data. Geological data include outcrop observations and seismic maps. If rock types and structural settings of the surface outcrops and subsurface formations are similar, outcrops can be regarded as relevant to the subsurface formation, and the statistical rules summarized from outcrop maps can constrain the model of subsurface formations. Seismic maps can provide information of large faults (at least tens of meters) due to their limited resolution. However, the associated small-scale damage zones around the fault can be estimated based on the self-similarity of fault segments and statistical distributions of inner and outer damage zones (Kim et al., 2004; De Joussineau and Aydin, 2007). Geomechanical data include current stress states and stress histories. The current stress state is essential for identifying the critically stressed natural fractures, while stress histories can further constrain the fracture properties, such as fracture orientations and sealing degrees. The other aspect is to find the appropriate failure criterion for particular formations. For example, differ-

ent rock types for different reservoirs should be considered, such as shale and granite for shale gas reservoirs and geothermal systems. The thermal impact on the failure of a specific rock type can also be significant due to the large temperature difference between the injected fluid and formation rocks. Interactions between fractures are neglected, considering the computation cost in this work. However, this impact is significant if fractures are close to each other, especially for formations with abundant natural fractures. In addition, global and local stress states can significantly change the hydraulic aperture and impact fracture conductance.

A potential application of this work is to estimate the size of SRV and predict shale gas production in an accurate and physically meaningful way. Production prediction is one of the essential issues in shale gas development. However, in currently available methods, such as empirical methods (Arps, 1945), analytical methods (Clarkson and Pedersen, 2010) and numerical simulation methods (Shabro et al., 2011), detailed SRV structures are neglected or significantly simplified, which brings enormous uncertainties on the results and difficulties in analyzing sensitivities. After optimizing the model with the two aspects mentioned above and combining existing SRV estimation methods, such as microseismic monitoring and electromagnetic imaging, this work provides detailed procedures to construct realistic structures of the subsurface formation and identify SRV under a given stress state. With the realistic SRV configuration and appropriate up-scaling methods, the numerical simulation or analytical solutions (Patzek et al., 2013) on a reservoir scale is possible and can be optimized to be more physically meaningful. The knowledge on influential factors from this work can further guide the history match of production data and analyze the well performance.

5. Conclusions

In this work, we mimic typical 2D and 3D formations with a stochastic discrete fracture network modelling method. By implementing the JRC-JCS failure criterion, we identify the SRV under a given stress state. We further systematically investigate the impact of different fracture properties on the formation and development of SRV. The fracture properties include geometrical properties (fracture lengths, center positions, and fracture orientations), mechanical properties (fracture roughness and strength), fracture sealing properties (the probability of open fractures and the segment length) and fracture intensity. Key conclusions are summarized below.

- Critically stressed fractures compose the backbone of SRV. Partially open fractures can enlarge the size of SRV by connecting more critically orientated fractures and contribute to the production significantly.

- For the total length (area in 3D) of critically stressed fractures, mechanical properties (fracture roughness (JRC) and strength (JCS)) and fracture orientations (κ) are the most important factors. Geometrical properties (fracture length (a) and center positions (F_D)) are important for SRV in 2D fracture networks, but insignificant in 3D fracture networks.

- For the total length of critically stressed fractures plus partially open fractures and the relative increase of SRV in 2D fracture networks, the probability of open fractures (P_o), fracture length (a), and center positions (F_D) are the most important factors. For 3D fracture networks, the probability of open fractures (P_o), the fracture intensity (FI) and fracture orientation (κ) are the essential factors.

- SRV formed in 2D fracture networks are sensitive to fracture lengths (a) and positions of fracture centers (F_D), but SRV formed in 3D fracture

networks are insensitive to these geometrical properties. Real fracture networks are always three-dimensional instead of two dimensional. Therefore, to accurately estimate SRV or have a good production prediction, it is particularly important to accurately assess the fracture sealing degree, fracture intensity, and fracture orientations of the subsurface fracture networks.

Declaration of competing interest

The authors report no conflicts of interest. The authors alone are responsible for the content and writing of this article.

Acknowledgements

This project was supported by the National Key Research and Development Program of China (No. 2019YFA0708704). The authors would like to thank Dr X. Li from Ennosoft for providing the UNCONG simulator to validate our cases.

Data Availability

All the data are generated by the in-house built DFN modelling software, HatchFrac. The C++ code of important algorithms are available online (Zhu et al., 2021d)(`https://data.mendeley.com/datasets/zhs97tsdry/1`)

References

Abouelresh, M.O., Babalola, L.O., 2020. 2d spatial analysis of the natural fractures in the organic-rich qusaiba shale outcrop, nw saudi arabia. J. Pet. Sci. Eng. 186, 106780.

Albright, J.N., Pearson, C.F., et al., 1982. Acoustic emissions as a tool for hydraulic fracture location: experience at the Fenton Hill hot dry rock site. SPE J. 22, 523–530.

Arps, J.J., 1945. Analysis of decline curves. Trans. AIME 160, 228–247.

Astakhov, D., Roadarmel, W., Nanayakkara, A., 2012. A new method of characterizing the stimulated reservoir volume using tiltmeter-based surface microdeformation measurements, in: SPE Hydraulic Fracturing Technology Conference, OnePetro.

Barton, C.A., Zoback, M.D., Moos, D., 1995. Fluid flow along potentially active faults in crystalline rock. Geology 23, 683–686.

Barton, N., 1973. Review of a new shear-strength criterion for rock joints. Eng. Geol. 7, 287–332.

Barton, N., Bandis, S.C., 1990. Review of predictive capabilities of jrc-jcs model in engineering practice, in: Proe. Int. Conf. Rock Joints., pp. 603–610.

Barton, N., Choubey, V., 1977. The shear strength of rock joints in theory and practice. Rock Mech. 10, 1–54.

Bello, R.O., Wattenbarger, R.A., et al., 2010. Multi-stage hydraulically fractured horizontal shale gas well rate transient analysis, in: North Africa technical conference and exhibition, Society of Petroleum Engineers.

Bonnet, E., Bour, O., Odling, N.E., Davy, P., Main, I., Cowie, P., Berkowitz, B., 2001. Scaling of fracture systems in geological media. Rev. Geophys. 39, 347–383.

Bour, O., Davy, P., 1997. Connectivity of random fault networks following a power law fault length distribution. Water Resour. Res. 33, 1567–1583.

Clarkson, C.R., Pedersen, P.K., 2010. Tight oil production analysis: adaptation of existing rate-transient analysis techniques, in: Canadian Unconventional Resources and International Petroleum Conference, OnePetro.

COULOMB, C., 1773. Essai sur une application des regles de maximis et minimis a quelques problemes de statique relatifs a 1'architecture. Mem. Div. Sav. Acad. .

Darcel, C., Bour, O., Davy, P., De Dreuzy, J., 2003. Connectivity properties of two-dimensional fracture networks with stochastic fractal correlation. Water Resour. Res. 39.

De Joussineau, G., Aydin, A., 2007. The evolution of the damage zone with fault growth in sandstone and its multiscale characteristics. J. Geophys. Res.: Solid Earth 112.

Dershowitz, W.S., 1984. Rock joint systems. Ph.D. thesis. Massachusetts Institute of Technology.

Ellefsen, K.J., Hsieh, P.A., Shapiro, A.M., 2002. Crosswell seismic investigation of hydraulically conductive, fractured bedrock near mirror lake, new hampshire. J. Appl. Geophys. 50, 299–317.

Fisher, M., Heinze, J., Harris, C., Davidson, B., Wright, C., Dunn, K., et al., 2004. Optimizing horizontal completion techniques in the Barnett shale using microseismic fracture mapping, in: SPE Annual Technical Conference and Exhibition, Society of Petroleum Engineers.

Fisher, M.K., Wright, C.A., Davidson, B.M., Goodwin, A., Fielder, E., Buckler, W., Steinsberger, N., et al., 2002. Integrating fracture mapping technologies to optimize stimulations in the Barnett Shale, in: SPE annual technical conference and exhibition, Society of Petroleum Engineers.

Haider, S., Saputra, W., Patzek, T., 2020. The key factors that determine the economically viable, horizontal hydrofractured gas wells in mudrocks. Energies 13, 2348.

Im, K., Elsworth, D., Fang, Y., 2018. The influence of preslip sealing on the permeability evolution of fractures and faults. Geophys. Res. Lett. 45, 166–175.

IM, S., 1993. Sensitivity estimates for nonlinear mathematical models. Math. Model. Comput. Exp 1, 407–414.

Jing, L., Stephansson, O., 2007. The Basics of Fracture System Characterization–Field Mapping and Stochastic Simulations, in: Developments in Geotechnical Engineering. Elsevier. volume 85, pp. 147–177.

Kemeny, J., Post, R., 2003. Estimating three-dimensional rock discontinuity orientation from digital images of fracture traces. Comput. Geosci. 29, 65–77.

Kim, Y.S., Peacock, D.C., Sanderson, D.J., 2004. Fault damage zones. J. Struct. Geol. 26, 503–517.

LaBrecque, D., Brigham, R., Denison, J., Murdoch, L., Slack, W., Liu, Q.H., Fang, Y., Dai, J., Hu, Y., Yu, Z., et al., 2016. Remote imaging of proppants in hydraulic fracture networks using electromagnetic methods: Results of small-scale field experiments, in: SPE Hydraulic Fracturing Technology Conference, OnePetro.

Lander, R., Laubach, S., 2015. Insights into rates of fracture growth and sealing from a model for quartz cementation in fractured sandstones. Bulletin 127, 516–538.

Laubach, S., Reed, R., Olson, J., Lander, R., Bonnell, L., 2004. Coevolution of

crack-seal texture and fracture porosity in sedimentary rocks: cathodoluminescence observations of regional fractures. J. Struct. Geol. 26, 967–982.

Lei, Q., Latham, J.P., Tsang, C.F., 2017. The use of discrete fracture networks for modelling coupled geomechanical and hydrological behaviour of fractured rocks. Comput. Geotech. 85, 151–176.

Li, X., Zhang, D., Li, S., 2015. A multi-continuum multiple flow mechanism simulator for unconventional oil and gas recovery. J. Nat. Gas Sci. Eng. 26, 652–669.

Liu, X., Jin, Y., Lin, B., 2021. An efficient stimulated reservoir area (sra) estimation method based on octree decomposition of microseismic events. J. Pet. Sci. Eng. 198, 108291.

Marder, M., Chen, C.H., Patzek, T., 2015. Simple models of the hydrofracture process. Phys. Rev. E 92, 062408.

Marelli, S., Sudret, B., 2014. Uqlab: A framework for uncertainty quantification in matlab, in: Vulnerability, uncertainty, and risk: quantification, mitigation, and management, pp. 2554–2563.

Marinos, V., Marinos, P., Hoek, E., 2005. The geological strength index: applications and limitations. Bull. Eng. Geol. Environ. 64, 55–65.

Mattila, J., Follin, S., 2019. Does In Situ State of Stress Affect Fracture Flow in Crystalline Settings? J. Geophys. Res.: Solid Earth 124, 5241–5253.

Maulianda, B., Hareland, G., Chen, S., 2014. Geomechanical consideration in stimulated reservoir volume dimension models prediction during multi-stage hydraulic fractures in horizontal wells–glauconite tight formation in hoadley field, in: 48th US rock mechanics/geomechanics symposium, OnePetro.

694 Maxwell, S.C., Urbancic, T., Steinsberger, N., Zinno, R., et al., 2002. Microseis-
695 mic imaging of hydraulic fracture complexity in the barnett shale, in: SPE
696 annual technical conference and exhibition, Society of Petroleum Engineers.

697 Maxwell, S.C., Waltman, C., Warpinski, N.R., Mayerhofer, M.J., Boroumand,
698 N., et al., 2009. Imaging seismic deformation induced by hydraulic fracture
699 complexity. SPE Reservoir Eval. Eng 12, 48–52.

700 Mayerhofer, M.J., Lolon, E., Warpinski, N.R., Cipolla, C.L., Walser, D.W.,
701 Rightmire, C.M., et al., 2010. What is stimulated reservoir volume? SPE
702 Prod.Oper. 25, 89–98.

703 Meakin, P., 1991. Invasion percolation on substrates with correlated disorder.
704 Physica A 173, 305–324.

705 Patzek, T.W., Male, F., Marder, M., 2013. Gas production in the barnett shale
706 obeys a simple scaling theory. PNAS 110, 19731–19736.

707 Prioul, R., Jocker, J., 2009. Fracture characterization at multiple scales using
708 borehole images, sonic logs, and walkaround vertical seismic profile. AAPG
709 Bull. 93, 1503–1516.

710 Raterman, K.T., Farrell, H.E., Mora, O.S., Janssen, A.L., Gomez, G.A., Busetti,
711 S., McEwen, J., Friehauf, K., Rutherford, J., Reid, R., et al., 2018. Sampling
712 a stimulated rock volume: An eagle ford example. SPE Reservoir Eval. Eng
713 21, 927–941.

714 Ren, L., Su, Y., Zhan, S., Hao, Y., Meng, F., Sheng, G., 2016. Modeling and
715 simulation of complex fracture network propagation with srv fracturing in
716 unconventional shale reservoirs. J. Nat. Gas Sci. Eng. 28, 132–141.

717 Rijks, E., Jauffred, J., 1991. Attribute extraction: An important application in
718 any detailed 3-d interpretation study. The Leading Edge 10, 11–19.

719 Rutledge, J.T., Phillips, W.S., 2003. Hydraulic stimulation of natural fractures
720 as revealed by induced microearthquakes, Carthage Cotton Valley gas field,
721 east TexasHydraulic Stimulation of Natural Fractures. Geophysics 68, 441–
722 452.

723 Shabro, V., Torres-Verdin, C., Javadpour, F., 2011. Numerical simulation of
724 shale-gas production: from pore-scale modeling of slip-flow, knudsen diffusion,
725 and langmuir desorption to reservoir modeling of compressible fluid, in: North
726 American Unconventional Gas Conference and Exhibition, OnePetro.

727 Shaffner, J.T., Cheng, A., Simms, S., Keyser, E., Yu, M., et al., 2011. The ad-
728 vantage of incorporating microseismic data into fracture models, in: Canadian
729 Unconventional Resources Conference, Society of Petroleum Engineers.

730 Thomas, R.N., Paluszny, A., Zimmerman, R.W., 2017. Quantification of frac-
731 ture interaction using stress intensity factor variation maps. J. Geophys. Res.:
732 Solid Earth 122, 7698–7717.

733 Warpinski, N.R., Mayerhofer, M.J., Vincent, M.C., Cipolla, C.L., Lolon, E.,
734 et al., 2009. Stimulating unconventional reservoirs: maximizing network
735 growth while optimizing fracture conductivity. J. Can. Pet. Technol. 48, 39–
736 51.

737 Warpinski, N.R., Wolhart, S., Wright, C., et al., 2001. Analysis and prediction
738 of microseismicity induced by hydraulic fracturing, in: SPE Annual Technical
739 Conference and Exhibition, Society of Petroleum Engineers.

740 Whitaker, A.E., Engelder, T., 2005. Characterizing stress fields in the upper
741 crust using joint orientation distributions. J. Struct. Geol. 27, 1778–1787.

742 Wilt, M., Alumbaugh, D., Morrison, H., Becker, A., Lee, K.H., Deszcz-Pan, M.,

1995. Crosswell electromagnetic tomography: System design considerations and field results. Geophysics 60, 871–885.

Wu, K., Olson, J.E., 2016. Numerical investigation of complex hydraulic-fracture development in naturally fractured reservoirs. SPE Prod.Oper. 31, 300–309.

Wu, S., Li, T., Ge, H., Wang, X., Li, N., Zou, Y., 2019. Shear-tensile fractures in hydraulic fracturing network of layered shale. J. Pet. Sci. Eng. 183, 106428.

Zhang, B., Tian, X., Ji, B., Zhao, J., Zhu, Z., Yin, S., 2019. Study on micro-seismic mechanism of hydro-fracture propagation in shale. J. Pet. Sci. Eng. 178, 711–722.

Zhu, W., He, X., Khirevich, S., Patzek, T.W., 2021a. Fracture sealing and its impact on the percolation of subsurface fracture networks. Earth and Space Science Open Archive , 30URL: https://doi.org/10.1002/essoar.10508231.1, doi:10.1002/essoar.10508231.1.

Zhu, W., He, X., Patzek, T.W., 2021b. Insights into the coupled effects of fracture geometry and sealing on stimulated reservoir volume in shales, in: 3rd International Discrete Fracture Network Engineering Conference, OnePetro.

Zhu, W., He, X., Santoso, R.K., Lei, G., Patzek, T., Wang, M., 2021c. Enhancing fracture network characterization: A data-driven, outcrop-based analysis. Earth and Space Science Open Archive , 35URL: https://doi.org/10.1002/essoar.10508232.1, doi:10.1002/essoar.10508232.1.

Zhu, W., Khirevich, S., Patzek, T., 2018. Percolation properties of stochastic fracture networks in 2d and outcrop fracture maps, in: 80th EAGE Conference and Exhibition 2018, European Association of Geoscientists & Engineers. pp. 1–5.

Zhu, W., Khirevich, S., Patzek, T.W., 2021d. Hatchfrac: A fast open-source dfn modeling software. Earth and Space Science Open Archive , 44URL: https://doi.org/10.1002/essoar.10508657.1, doi:10.1002/essoar.10508657.1.

Zhu, W., Khirevich, S., Patzek, T.W., 2021e. Impact of fracture geometry and topology on the connectivity and flow properties of stochastic fracture networks. Water Resour. Res. , e2020WR028652.

Zhu, W., Lei, G., He, X., Yang, Y., Santoso, R.K., Wang, M., 2021f. Are natural fractures pervasive? Earth and Space Science Open Archive , 46URL: https://doi.org/10.1002/essoar.10508401.1, doi:10.1002/essoar.10508401.1.